NASA Technical Memorandum 84598

STRAIN ENERGY RELEASE RATE ANALYSIS
OF CYCLIC DELAMINATION GROWTH IN
COMPRESSIVELY LOADED LAMINATES
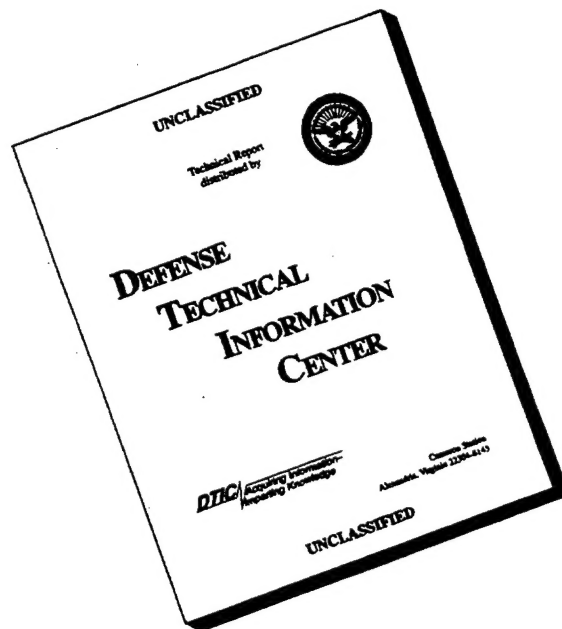
John D. Whitcomb

January 1983

19951226 089

NASA
National Aeronautics and
Space Administration

Langley Research Center
Hampton, Virginia 23665

DTIC QUALITY INSPECTED 3

DISCLAIMER NOTICE

UNCLASSIFIED

Technical Report
distributed by

**DEFENSE
TECHNICAL
INFORMATION
CENTER**

DTIC Acquiring Information
Imparting Knowledge

Cameron Station
Alexandria, Virginia 22304-6145

UNCLASSIFIED

THIS DOCUMENT IS BEST QUALITY AVAILABLE. THE COPY FURNISHED TO DTIC CONTAINED A SIGNIFICANT NUMBER OF PAGES WHICH DO NOT REPRODUCE LEGIBLY.

```
  5   OF     6
 --                        ***DTIC DOES NOT HAVE THIS ITEM***
 -- 1 -   AD NUMBER: D437176
 -- 5 -   CORPORATE AUTHOR: NATIONAL AERONAUTICS AND SPACE ADMINISTRATION
 --       HAMPTON VA LANGLEY RESEARCH CENTER
 -- 6 -   UNCLASSIFIED TITLE:     STRAIN ENERGY RELEASE RATE ANALYSIS OF
 --       CYCLIC DELAMINATION GROWTH IN COMPRESSIVELY LOADED LAMINATES.
 --10 -   PERSONAL AUTHORS: WHITCOMB,J. D. ;
 --11 -   REPORT DATE:      JAN   , 1983
 --12 -   PAGINATION:       39P
 --14 -   REPORT NUMBER:    NASA-TM-84598
 --20 -   REPORT CLASSIFICATION:  UNCLASSIFIED
 --22 -   LIMITATIONS (ALPHA):    APPROVED FOR PUBLIC RELEASE; DISTRIBUTION
 --       UNLIMITED. AVAILABILITY: NATIONAL TECHNICAL INFORMATION SERVICE,
 --       SPRINGFIELD, VA. 22161. N83-17599.
 --33 -   LIMITATION CODES:  1  24
```

STRAIN ENERGY RELEASE RATE ANALYSIS OF CYCLIC DELAMINATION GROWTH IN COMPRESSIVELY LOADED LAMINATES

John D. Whitcomb
NASA Langley Research Center
Hampton, Virginia 23665

SUMMARY

Delamination growth in compressively loaded composite laminates was studied analytically and experimentally. The configuration used in the study was a laminate with an across-the-width delamination. An approximate superposition stress analysis was developed to quantify the effects of various geometric, material, and load parameters on mode I and mode II strain energy release rates G_I and G_{II}, respectively. Calculated values of G_I and G_{II} were then compared with measured cyclic delamination growth rates to determine the relative importance of G_I and G_{II}. High growth rates were observed only when G_I was large. However, slow growth was observed even when G_I was negligibly small. This growth apparently was due to a large value of G_{II} ((AUTHOR))

INTRODUCTION

In composite structures subjected to compression loads, delaminations can cause localized buckling (fig. 1). High interlaminar stresses at the edges of the buckled region often lead to cyclic delamination growth (herein referred to as instability-related delamination growth).

The objective of this paper is to investigate the mechanism of instability-related delamination growth. Figure 1 shows the configuration used in the study--a laminate with a "through-width" delamination. This configuration was selected because it is perhaps the simplest configuration that exhibits instability-related delamination growth. Goals of the investigation were: (1) to develop and use an approximate superposition stress analysis to explain how various geometric, material, and load parameters affect interlaminar stresses, (2) to determine the delamination growth behaviors predicted by several different criteria based on strain energy release rates, and (3) to

compare analytical calculations with experimental observations to determine the applicability of each growth criterion.

Because of the stress singularity at the end of the delamination (crack tip), calculated stresses there have little meaning. Strain energy release rates are finite parameters which characterize the intensity of the stresses near the crack tip. Consequently, in the following discussion strain-energy release rates will be used to characterize the severity of the interlaminar stresses.

NOMENCLATURE

a	half-length of delamination before loading
$\bar{a}$	half-length of delamination after loading
Δa	virtual crack closure distance used in strain energy release rate calculations
b	specimen width
C, C1, C2, C3, n, n1, n2, Z	arbitrary constants
D	bending stiffness of the buckled region given by

$$D = \frac{b}{3} \sum_{k=1}^{\rho} E^k \left[\left(\alpha_k - \frac{t}{2} \right)^3 - \left(\alpha_{k-1} - \frac{t}{2} \right)^3 \right]$$

where ρ = number of plies

d_x, d_y	unit load solutions for displacements near crack tip
E^k	Young's modulus for ply k
E_{11}, E_{22}, E_{33}	Young's moduli of unidirectional ply. The subscripts 1, 2, and 3 refer to the longitudinal, transverse, and thickness directions respectively.

2

F_x, F_y	unit load solutions for forces at crack tip
G_I	Mode I strain-energy release rate
G_{II}	Mode II strain-energy release rate
$\hat{G}_I$	maximum possible value of G_I for current delamination length
G_{12}, G_{13}, G_{23}	shear moduli of unidirectional ply
M	moment
N	number of applied load cycles
P_A, P_B, P_C, P_D	axial loads in regions A, B, C, and D respectively
P_T	remote applied compressive load
S_A, S_B, S_C, S_D	axial stiffness of regions A, B, C and D given by

$$S = b \sum_{k=1}^{\rho} E^k (\alpha_k - \alpha_{k-1})$$

where ρ = number of plies

t	thickness of buckled region
x, y	rectangular Cartesian coordinates
α_{k-1}	distance from top surface of laminate to ply "k"; top ply is ply 1
δ	lateral deflection at $x = -a$ due to applied load
$\hat{\delta}$	value of δ corresponding to $\hat{G}_I$
δ_o	initial lateral deflection at $x = -a$
ν_{12}, ν_{13}, ν_{23}	Poisson's ratios for unidirectional ply

ANALYSIS

The configuration shown in figure 1 was idealized as a two dimensional plane strain problem. Linear and nonlinear finite element analyses and an approximate superposition analysis were used to calculate strain energy release rates for the two dimensional idealization. The nonlinear analysis was used to provide reference solutions for evaluation of the approximate superposition analysis. The linear analysis was used to calculate several constants used in the approximate superposition analysis. The nonlinear analysis is described in reference 2, and the linear analysis is simply a linear version of this analysis.

The approximate superposition analysis, the procedure for calculating strain energy release rates, the finite element models, and material properties are discussed in the following sections.

Approximate Superposition Analysis

Superposition techniques have been widely used in linear stress analysis to represent a complicated problem as a combination of several simpler problems. Application of the principle of superposition to nonlinear problems first requires a transformation that results in a linear system.

The key to the transformation is replacement of the source of nonlinearity with equivalent loads (fig. 2a and b). Because of symmetry only half of the configuration is considered. The buckled region (which responds nonlinearly due to significant rotations) is replaced by the loads P_D and M, the axial load and moment respectively in the column where it is cut (fig. 2b). The new configuration is linear, with three nonlinearly related applied loads P_T, P_D, and M. By superposition the number of loads can be reduced to two, as illustrated in figures 2c - 2e.

4

The load system in figure 2c is divided into the two load systems shown
in figures 2d and 2e. Because P_C is calculated using rule of mixtures,
the load system in figure 2e causes a uniform axial strain state and no inter-
laminar stresses. Consequently, in terms of interlaminar stresses, only the
load system in figure 2d (ie. (P_C-P_D) and M) need be considered. Accordingly,
in the current study involving strain energy release rates, figure 2d is
the linearized equivalent of the nonlinear problem in figure 2a.

The appendix describes a strength of materials analysis for calculating
$(P_C - P_D)$ and M. The key equations from the appendix are

$$P_T = \frac{\pi^2 S_A}{a^2} \left[\frac{(\delta^2 + 2\delta\delta_o)}{16} + \frac{D(S_A + S_D)}{S_A S_D} \frac{\delta}{\delta + \delta_o} \right] \tag{1}$$

$$P_C - P_D = \frac{S_D}{S_A + S_D} P_T - \frac{\pi^2 D}{a^2} \frac{\delta}{\delta + \delta_o} \tag{2}$$

$$M = \frac{\pi^2 D}{2a^2} \delta \tag{3}$$

To use the loads $(P_C - P_D)$ and M in a two dimensional analysis requires that
they be expressed as an equivalent distribution of tractions. To calculate
this distribution, the axial strains were assumed to vary linearly through the
thickness where the tractions are applied (ie. at the cut). Intuitively, this
seems to be reasonable if region D (fig. 2) is not cut too close to the
crack tip. The validity of the assumed linear variation will be checked later
in this paper.

Linear finite element analysis was used to calculate the response of the
linearized configuration in figure 2d to unit values of $(P_C - P_D)$ and M.
Because the configuration is linear, the solution for any arbitrary combination

of $(P_C - P_D)$ and M is simply a linear combination of the unit load responses. If region B (fig. 2) is much thicker than region C, the unit load solutions are very insensitive to delamination length. In the current study the ratio of thicknesses was 61 to 3. Hence, the unit load solutions for $2a = 25$ mm were used for analysing all delamination lengths. Also initial waviness of the buckled region does not enter into the finite element analysis. Delamination length and initial waviness were both accounted for in the strength of materials analysis in calculating $(P_C - P_D)$ and M, equations (2) and (3) respectively. This procedure will be discussed further in the next section.

Strain Energy Release Rate

The virtual crack closure method (ref. 1) was used to calculate mode I and mode II strain-energy release rates, G_I and G_{II} respectively. The forces transmitted through the node at the crack tip and the relative displacements of the two nodes on the crack boundary closest to the crack tip were used in the calculation. Equations 4 show how this technique is used for the super-position stress analysis.

$$G_I = \frac{1}{2\Delta ab} \left[(P_C - P_D)F_y^1 + MF_y^2 \right] \left[(P_C - P_D)d_y^1 + Md_y^2 \right]$$

$$G_{II} = \frac{1}{2\Delta ab} \left[(P_C - P_D)F_x^1 + MF_x^2 \right] \left[(P_C - P_D)d_x^1 + Md_x^2 \right]$$

(4)

In these equations F_x, F_y, d_x, and d_y are the unit load values of the nodal forces and the corresponding relative nodal displacements in the x and y directions. (The coordinate system is defined in fig. 2.) The superscripts 1 and 2 on the unit load parameters identify parameters associated with $(P_C - P_D)$ and M, respectively.

6

If the distance is small between the crack tip and the nodes used to calculate relative displacements, then $F_y^1/d_y^1 = F_y^2/d_y^2$ and $F_x^1/d_x^1 = F_x^2/d_x^2$. Using these relationships in eqns. (4) results in

$$G_I = \frac{1}{2\Delta ab} \frac{d_y^1}{F_y^1} \left[(P_C - P_D)F_y^1 + MF_y^2 \right]^2$$

$$(5)$$

$$G_{II} = \frac{1}{2\Delta ab} \frac{d_x^1}{F_x^1} \left[(P_C - P_D)F_x^1 + MF_x^2 \right]^2$$

In the results and discussion section it will be shown that for high loads or long delamination lengths, G_I is zero, i.e., the crack tip closes in the normal direction. To prevent the crack faces from overlapping (analytically) requires the addition of multipoint constraints on the crack face nodes. Conceptually, the crack face nodes are connected in the direction normal to the crack face by infinitesimal springs. These springs have infinite stiffness in compression and zero stiffness in tension. To determine whether to select zero or infinite stiffness requires solution of a non near contact problem. To include the contact problem directly in the superposition analysis would severely complicate the otherwise simple equations. Therefore, use of a non-contact analysis to approximate G_{II} was investigated.

A laminate with $2a = 76.2$ mm was analyzed using two different approaches. First contact forces were ignored (i.e., overlap of crack faces was allowed). G_I and G_{II} were calculated using equation (5). In the second approach, overlap of the crack faces was prevented, which is more realistic. G_{II} was calculated using equation (5). (Note that eq. (5) yeilds $G_I = 0$ when overlap is prevented.) Applied loads (P_T) ranged from 14.8 kN, which corresponds approximately to initial crack tip closure, to 55.2 kN.

7

When crack face overlap was prevented, a larger value of G_{II} was calculated than when overlap was allowed. The difference in the G_{II} values increased with load. But in all cases the difference was approximately equal to G_I calculated using the approach which allowed crack face overlap. For example, for $P_T = 55.2$ kN the contact analysis yielded $G_{II} = 413$ J/m^2. When crack face overlap was allowed, G_I and G_{II} were 35 and 384 J/m^2, respectively. The sum of these values is within approximately 1.5 percent of the more realistic solution, i.e., $G_{II} = 413$ J/m^2. Apparently the crack-face contact forces do not significantly alter the total strain energy release rate. Hence, when there is crack tip closure, the total strain energy release rate from the non-contact analysis can be used to approximate G_{II} (which is then the total strain energy release rate, since G_I is identically zero).

Finite Element Model

A typical finite element mesh for the nonlinear analysis is shown in figure 3. Because of symmetry only half of the laminate was modeled. The mesh contains 813 nodes and 740 four-node isoparametric elements. Reduced integration was used to improve the performance of the elements in modeling bending deformations. Because the rotations are small except in part of the buckled region, the nonlinear strain-displacement relations were used only for the region $y > 0$, $-a \leq x \leq -0.56$ mm. As shown in figure 2(b), the linearized configuration is the same as the nonlinear configuration except that most of the buckled region is removed. Accordingly, the mesh used in the linear analysis was derived from that in figure 3 by removing elements in the deleted part of the buckled region.

8

Materials Properties

The material studied was NARMCO T300/5203* graphite/epoxy. The unidirectional ply properties were assumed to be

$$E_{11} = 140 \text{ GPa}$$

$$E_{22} = E_{33} = 14 \text{ GPa}$$

$$\nu_{12} = \nu_{13} = \nu_{23} = 0.21$$

$$G_{12} = G_{13} = G_{23} = 5.9 \text{ GPa}$$

Plane strain (i.e., $\epsilon_z = 0$) and $\epsilon_{xz} = 0$ were imposed to calculate the 2D properties. In regions where coarse finite elements spanned several plies, laminate theory was used to obtain average properties.

---

*Use of trade names or manufacturers does not constitute an official endorsement, either expressed or implied, by the National Aeronautics and Space Administration.

EXPERIMENTAL PROCEDURE

The specimens used for this study were fabricated and tested by Northrop Corporation. (Details will appear in NASA CR-166046, "Performance of a Quantitative Study of Instability-Related Delamination Growth," by R. L. Ramkumar.) A cursory description of the experimental procedure is given herein.

The specimen consisted of 64 plies of T300/5208. The fiber orientation and stacking sequence were $[0_4/(0/45/90/-45)_7]_s$. The laminate width, b, was 25.4 mm To simulate a delamination, kapton film was used to prevent bonding over a 19 mm length between the third and fourth plies. The ply thickness was assumed to be 0.14 mm. Six specimens were tested in fatigue under compressive constant-amplitude loads. Minimum compressive load was ten percent of the maximum compressive load. The load frequency was 10 Hz. Delamination lengths were measured with a microscope.

RESULTS AND DISCUSSION

First, the accuracy of the approximate superposition analysis will be evaluated. Then the effect of various parameters on G_I and G_{II} will be considered. Finally, the experimental observations will be compared with the analytical results.

Evaluation of Approximate Superposition Analysis

The approximate superposition analysis was evaluated by comparison with results from a geometrically nonlinear finite element analysis. Recall that a major assumption in the approximate analysis was that the strains vary linearly through the thickness where $(P_C - P_D)$ and M are applied. Fig. 4 shows the axial strain variation through the thickness at $x = -0.2$ and -0.7 mm obtained using the nonlinear finite element analysis. Along the line $x = -0.7$ mm the strains vary almost linearly for the three applied loads. However, closer to the crack tip along $x = -0.2$ mm the variation is more nonlinear, especially

near $y = 0$. In the following, $(P_C - P_D)$ and M were applied at $x = -0.76$ mm.

The unit load solutions F_x, F_y, d_x, and d_y are

$$F_x^1 = 9.36 \times 10^{-5}$$

$$F_x^2 = 0.531 \text{ m}^{-1}$$

$$F_y^1 = 0.0261$$

$$F_y^2 = -0.252 \text{ m}^{-1}$$

$$d_x^1 = 1.40 \times 10^{-10} \text{ m-N}^{-1}$$

$$d_y^1 = 1.17 \times 10^{-8} \text{ N}^{-1}$$

These values were used in equation 5 for any combination of $(P_C - P_D)$ and M to obtain G_I and G_{II}.

Differences between G_I and G_{II} from the approximate superposition analysis and the geometrically nonlinear finite element analysis can be traced mainly to two sources: (1) nonlinear variation of the strains through the thickness of the buckled region and (2) inaccuracy in determining $(P_C - P_D)$ and M.

By using $(P_C - P_D)$ and M from the geometrically nonlinear finite element analysis, the effect of nonlinear variation of the strains can be examined. Figure 5 shows that this effect is small.

Figure 6 shows that if the strength of materials analysis is used to calculate $(P_C - P_D)$ and M, the difference is much larger. Hence, most of the difference between the two analyses is due to inaccuracy in determining $(P_C - P_D)$ and M. But the general trends for the G_I variation with delamination length and load are predicted very well. In figure 6 the curves for the two analyses seem to differ (approximately) by a constant scale factor.

A direct test of the approximate analysis for predicting trends is to use it to coalesce the curves in figure 6 into a single curve. Equations (2) and (3) show that $(P_C - P_D)$ and M can be expressed as functions of δ. Hence, from equations (5), G_I and G_{II} are functions of δ. Equations (1), (2), (3), and (5) show that for constant δ, P_T varies as a^{-2} and G_I and G_{II} vary as a^{-4}. Hence, plotting $a^4 G_I$ vs $a^2 P_T$ should coalesce the curves for various delamination lengths. Figure 7 shows that the data for five delamination lengths (including those in fig. 6) do coalesce into a narrow band around a single curve. Since the peak values of G_I for various lengths differ by more than two orders of magnitude, the closeness of the fit suggests the approximate analysis is accurate for predicting trends. Therefore, all results that follow are obtained with the approximate superposition analysis. Figure 7 also shows that if nonlinear finite element results are available for one delamination length, the values for other lengths can be estimated immediately.

An advantage of the superposition analysis is that it allows a problem to be dissected. In particular, one can determine the relative importance of the loads $(P_C - P_D)$ and M on G_I and G_{II}. Figures 8 and 9 show G_I and G_{II} calculated by using M alone and by using $(P_C - P_D)$ and M in combination. Although intuition might suggest that only the peeling action caused by the moment M has a significant effect on G_I, figure 8 shows that $(P_C - P_D)$ contributions cannot be ignored. Figure 9 shows that both $(P_C - P_D)$ and M are also important when calculating G_{II}.

Parametric Study

The effects of several parameters on G_I and G_{II} were examined using the approximate superposition analysis. The parameters were initial waviness,

delamination length, applied load, and the ratio of axial to bending stiffness for the buckled region.

Initial imperfections in the form of simple sinusoidal waviness were assumed (eq. (6))

$$v(x)\Big|_{INITIAL} = \frac{\delta_o}{2}\left(1 - \cos\frac{\pi x}{a}\right) \tag{6}$$

where $v(x)$ = Distortion in the y direction. When a column is initially wavy, bifurcation buckling does not occur. As soon as load is applied, the column begins to deflect laterally, which causes interlaminar stresses. Hence, G_I and G_{II} are nonzero as soon as load is applied. If $\delta_o = 0$, G_I and G_{II} are zero until buckling occurs. However, figure 10 shows that the peak value of G_I is significantly reduced, even for very small imperfections. In contrast, figure 11 shows that G_{II} is hardly affected by initial waviness.

Figures 6, 12, and 13 show the effect of delamination length on G_I and G_{II}. The shorter delaminations have the larger values of peak G_I (i.e., $\hat{G}_I$) (fig. 6). However, for the longer delaminations G_I becomes nonzero at lower loads. Figure 12 shows that after only a little delamination growth, G_I reaches a peak and decreases rapidly with further growth. At $2a = 40$-50 mm, the crack tip closes in the normal direction and G_I is identically zero. Further delamination growth causes compressive normal stresses to develop at the crack tip. In contrast, G_{II} initially increases then decreases only slightly to a constant value with increased delamination length (fig. 13). Note that G_{II} is typically much larger than G_I.

Figures 6 and 14 illustrate the effects of applied load on G_I and G_{II}, respectively. The mode I strain energy release rate G_I first increases to a peak value ($\hat{G}_I$), then decreases with increasing load (fig. 6). In contrast, G_{II} monotonically increases with increasing load. As a result, G_I and G_{II} do not usually reach peak values

13

at the same time during a fatigue load cycle. Furthermore, the load at which G_I is maximum decreases with increasing delamination length.

Since $\hat{G}_I$ is the maximum possible value of G_I for a given delamination length, it is of interest how $\hat{G}_I$ varies with delamination length. The first step in determining this variation is to determine the lateral deflection $\hat{\delta}$ corresponding to $\hat{G}_I$. The lateral deflection $\hat{\delta}$ is obtained by solving

$$\frac{\partial G_I}{\partial \delta} = 0 \tag{7}$$

Equations (2), (3), (5), and (7) are combined to obtain the governing equation (eq. (8))

$$d_y^1 \left[\frac{S_A S_D}{S_A + S_D} \frac{\hat{\delta}(1 + \delta_o)}{8} + \frac{D\delta_o}{(\hat{\delta} + \delta_o)^2} \frac{1 - S_A}{S_A} \right] + \frac{d_y^2 D}{2} = 0 \tag{8}$$

Equation (8) is solved iteratively for $\hat{\delta}$. Once $\hat{\delta}$ is determined, $\hat{G}_I$ can be calculated from equation (1), (2), (3), and (5). Note that $\hat{\delta}$ is independent of delamination length. Earlier it was shown that for constant δ, G_I and G_{II} vary as a^{-4} and P_T varies as a^{-2}. Hence, $\hat{G}_I$ varies as a^{-4} and the corresponding applied load varies as a^{-2}. The corresponding value of G_{II} also varies as a^{-4}. These observations will be of special interest later when examining the fatigue data.

The last parameter to be examined is the ratio of flexural-to-axial stiffness (i.e., D/S_D) of the delaminated region. The buckling load for the region is linearly related to D. Prior to buckling, the load in the delaminated region is linearly related to S_D. Hence, for thick specimens with a thin delaminated region the applied load which causes buckling depends on the ratio D/S_D. Delaminated regions are less prone to buckle if they possess low

14

axial stiffness and high flexural stiffness. But for homogeneous materials or unidirectional orthotropic laminates, this ratio is simply

$$\frac{D}{S_D} = \frac{t^2}{12} \tag{9}$$

Hence, the applied load which causes buckling is independent of the material properties of the buckled region. However, for multi-directional laminates the ratio D/S_D depends on both the lamina properties and the stacking sequence. For example, the value of S_D for a $[0_3]$ laminates is approximately 1.4 times that for a $[0/90/0]$ laminate, but the value of D is essentially the same for both laminates. Consequently, for a thick laminate with a delamination, buckling occurs at a lower applied load if the delaminated region is $[0_3]$ rather than $[0/90/0]$.

Comparison of Analysis and Fatigue Data

The roles of G_I and G_{II} in delamination growth were investigated by comparing calculated values of G_I and G_{II} with measured growth rates. Fatigue data for six specimens from reference 3 were used for comparison with analytical results. Three of the specimens were tested at $(P_T)_{max} = 33$ KN and another three at $(P_T)_{max} = 30$ KN. The results are presented in figure 15. $\frac{da}{dN}$ decreased rapidly with delamination growth. Both curves are approximately linear with a slope of -4, hence

$$\frac{da}{dN} \approx Ca^{-4} \tag{10}$$

Figure 16 shows $\frac{da}{dN}$ vs. the maximum values of G_I and G_{II} during fatigue cycling at a maximum compressive load of 33 KN. Note that the growth rate is largest when G_I is relatively large. But slow growth is observed

even when G_I is very small. The mode II strain energy release rate G_{II} changes little after initial delamination growth. Since G_{II} remains large, delamination growth likely is driven by G_{II}.

Two delamination growth criteria were examined to determine whether they could predict the observed growth rates. The first growth criterion examined is given by

$$\frac{da}{dN} = ZG_I^n \tag{11}$$

where Z and n are constants. Eqn. (11) is evaluated at the point in the load cycle when G_I is maximum. The load range and delamination lengths are such that for almost the entire test, the maximum G_I during each load cycle is $\hat{G}_I$, which was obtained by solving equation (7). Recognizing that $\hat{G}_I$ decreases as a^{-4}, as shown earlier, equations (10) and (11) can be solved for n; the result is $n = 1$. This is in strong contrast to published values of $n \approx 15$–20 for double cantilever beam fatigue tests (ref. 3). Apparently, equation (11) is not a valid growth criterion for the specimens considered.

Next a growth criterion was considered which includes both G_I and G_{II}. If we assume there is no synergistic interaction of G_I and G_{II} (i.e., the effects are separable), then

$$\frac{da}{dN} = f_1(G_I) + f_2(G_{II}) \tag{12}$$

where f_1 and f_2 are functions of G_I and G_{II} respectively.

From the double cantilever beam data just discussed, we know that f_1 is extremely sensitive to G_I $\left(\text{i.e., } \frac{da}{dN} \propto G_I^{15}\right)$. Since G_I decreases rapidly with increasing "a", f_1 must also decrease extremely fast as "a" increases. In fact, f_1 would not contribute noticeably to da/dN after

16

the initial growth. Hence delamination growth appears to be driven by G_{II} alone. Accordingly, it was assumed that the growth criterion should be evaluated when G_{II} is maximum, i.e., at peak load. However, earlier it was shown that for long delaminations the crack tip closes and produces compressive σ_y stresses when the cyclic load is maximum. The compressive stress probably reduces the effect of G_{II} on delamination growth, but it was not clear how to account for this stress. Two approaches were tried: (1) Ignore the compressive normal stress and set $f_1 = 0$ when the tip closes or (2) let f_1 take on negative values after the crack tip closes.

If we choose to set $f_1 = 0$ when the crack tip closes, then

$$\frac{da}{dN} = f_2(G_{II}) \tag{13}$$

for virtually the entire test. Figure 14 showed that G_{II} first increased then decreased slightly as the delamination extends. In the experiments two load levels were used: $(P_T)_{max} = 33$ KN and 30 KN. Figure 14 shows that for $2a > 25$ mm, the minimum value of G_{II} for $(P_T)_{max} = 33$ KN is greater than the maximum value of G_{II} for $(P_T)_{max} = 30$ KN. Hence, equation (13) would predict that for $2a > 25$ mm, the minimum da/dN for the higher load should exceed the maximum da/dN at the lower load. Figure 16 shows this is not the case. Hence, equation (13) is not valid.

If we select a function f_1 that becomes negative when the crack tip closes, then we (analytically) allow compressive normal stresses at the crack tip to retard delamination growth due to G_{II}. Since the compressive crack tip stresses increase as the delamination grows, such a function f_1 would predict a decrease in growth rate with increased delamination length. Although this prediction agrees with the data trend in figure 15, more tests are needed to verify or disprove this interpretation.

17

Despite the complexity of the growth behavior, two trends were clear: (1) high growth rates were observed only when G_I was large, and (2) slow growth was observed even when G_I was negligibly small; apparently, G_{II} alone can drive delamination growth.

CONCLUSIONS

Analysis and experiments were used to study instability-related delamination growth in a fatigue specimen with a through-width delamination. To perform the analysis an approximate superposition analysis was developed. The analysis expresses G_I and G_{II} in closed form, which can be used easily to determine the effects of various parameters. The analysis agreed very well with more rigorous solutions.

The response of the delaminated laminate to applied loads was found to be very complex. Key observations are listed below.

(1) G_{II} is generally much larger than G_I.

(2) G_I and G_{II} usually reach their peak magnitudes at different points in a fatigue cycle. G_{II} always reaches its peak value at maximum load.

(3) High delamination growth rates were accompanied by large values of G_I.

(4) Slow growth rates were observed even when G_I was negligibly small. This growth apparently was due to a large value of G_{II}.

APPENDIX

A strength of materials analysis is described herein for the configuration in figure 1.

The configuration is subdivided into four regions, as shown in figure 2. Because of symmetry, only half of the laminate is modeled. The laminate is of width b. The following assumptions are made:

1. Regions B and C are perfectly bonded. Regions A and D are unbonded.

2. Regions A, B, and C have constant axial strain. Hence, the force-displacement relations are those for a simple rod subjected to axial load.

3. Region D has zero slope at both ends.

4. Region D has an initial sinusoidal imperfection of peak magnitude δ_o. The initial shape is given by

$$v(x)\big|_{initial} = \frac{\delta_o}{2}\left(1 - \cos\frac{\pi x}{a} \right) \tag{A1}$$

where $v(x) =$ the distortion in the y direction.

To describe the nonlinear behavior of region D, equations (A2) and (A3) for post-buckling of a column were used.

$$P_D = \frac{\pi^2 D}{a^2}\frac{\delta}{\delta + \delta_o} \qquad\qquad \text{(ref. 4)} \tag{A2}$$

$$a - \bar{a} = \frac{\pi^2}{16a}\left(\delta^2 + 2\delta\delta_o\right) + \frac{aP_D}{S_D} \qquad \text{(ref. 5)} \tag{A3}$$

where δ, a, $\bar{a}$, and P_D are peak lateral deflection, axial length before and after deformation, and load, respectively. Equations (A2) and (A3) were derived using strength of materials analysis of a column.

19

To combine regions A, B, C, and D, equilibrium and compatibility conditions must be considered. The equilibrium condition for the axial force is

$$P_A + P_D = P_B + P_C = P_T \tag{A4}$$

Compatibility requires the shortening of regions A and D to be identical. Hence,

$$\frac{P_A a}{S_A} = a - \bar{a} \tag{A5}$$

Equations (A2) to (A5) can be combined to obtain the governing equation for the laminate.

$$P_T = \frac{\pi^2 S_A}{a^2} \left[\frac{1}{16} (\delta^2 + 2\delta\delta_o) + \frac{D(S_A + S_D)}{S_A S_D} \frac{\delta}{\delta + \delta_o} \right] \tag{A6}$$

For a specified load P_T, equation (A6) is solved using a Newton-Raphson technique to obtain δ. P_D can then be calculated using equation (A2). From static equilibrium, the moment acting on the delaminated region at the crack tip is

$$M = \frac{P_D}{2} (\delta + \delta_o) = \frac{\pi^2 D}{2a^2} \delta \tag{A7}$$

The force P_C is found from rule of mixtures as

$$P_C = \frac{S_D}{S_A + S_D} P_T \tag{A8}$$

20

REFERENCES

[1] Rybicki, E. F.; and Kanninen, M. F.: A Finite Element Calculation of Stress Intensity Factors by a Modified Crack Closure Integral. _Engineering Fracture Mechanics_, vol. 9, no. 4, 1977, pp. 931-938.

[2] Whitcomb, J. D.: Finite Element Analysis of Instability-Related Delamination Growth. _Journal of Composite Materials_, vol. 15, Sept. 1981, pp. 403-426.

[3] Wilkins, D. J.: A Comparison of the Delamination and Environmental Resistance of a Graphite-Epoxy and a Graphite-Bismaleimide. Naval Air Systems Command Report NAV-GD-0037, 1981.

[4] Brush, D. O.; and Almroth, B. L.: _Buckling of Bars, Plates, and Shells_. McGraw-Hill Book Co., Inc., New York, 1975, pp. 13-14.

[5] Ashizawa, M.: Fast Interlaminar Fracture of a Compressively Loaded Composite Containing a Defect. Presented at the Fifth DOD/NASA Conference on Fibrous Composites in Structural Design, New Orleans, LA, Jan. 1981. (Douglas Paper No. 6994.)
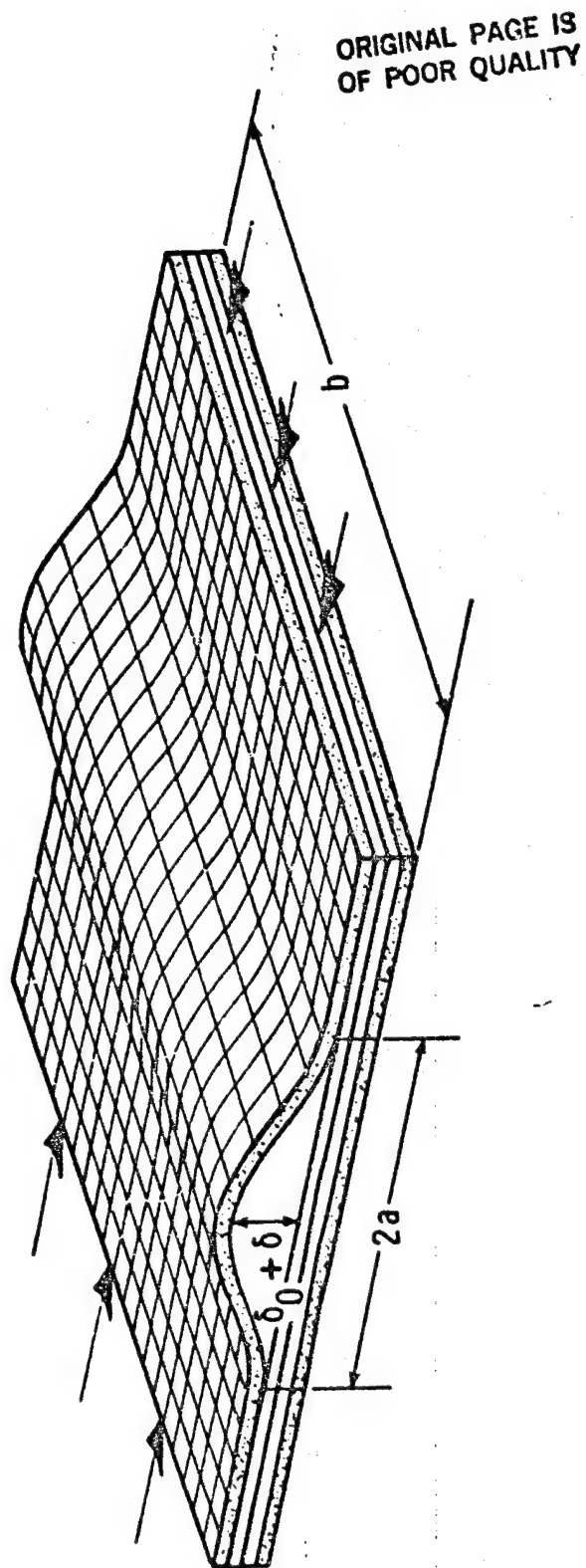
Fig. 1— Local buckling of laminate with through-width delamination.
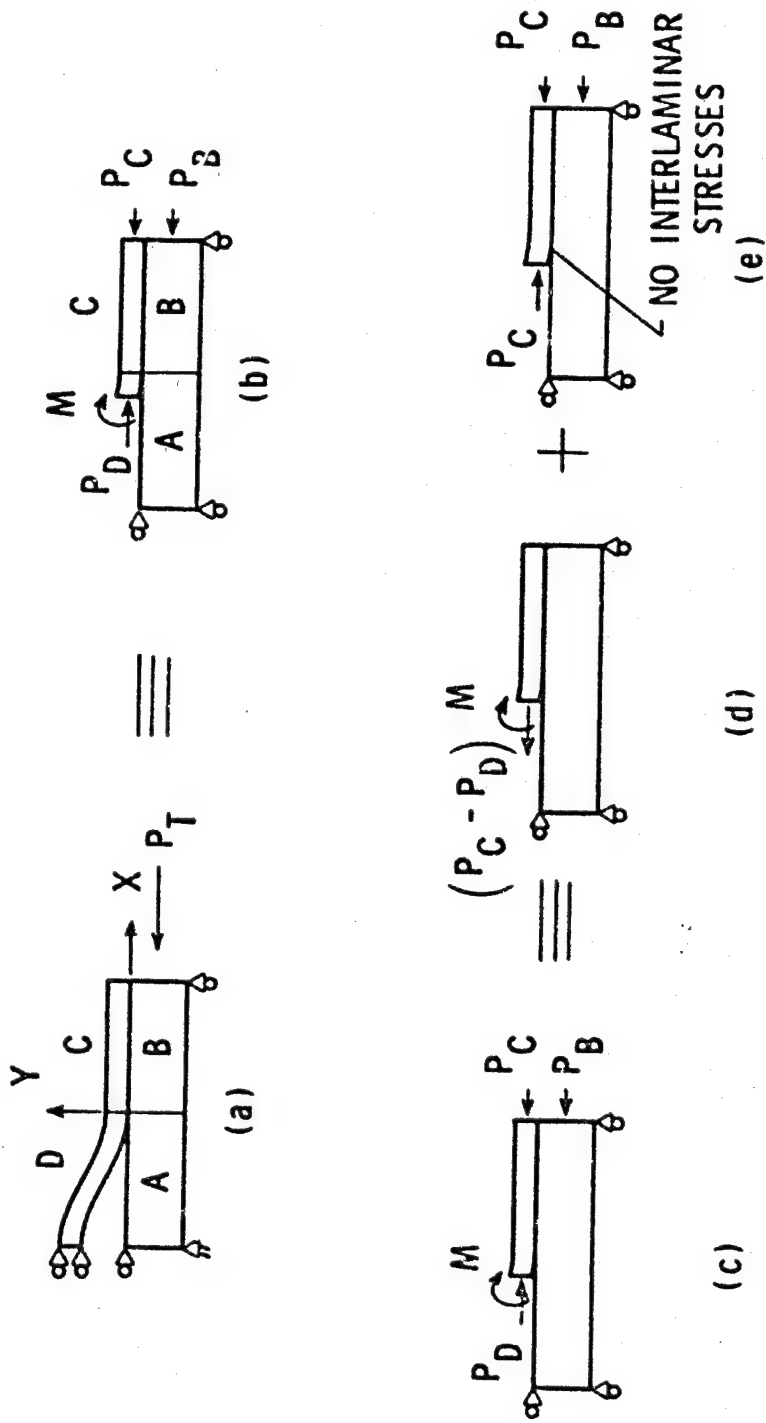
Fig. 2— Nonlinear configuration (a) transformed into linear configuration (d) with two nonlinearly related loads, $(P_C - P_D)$ and M.
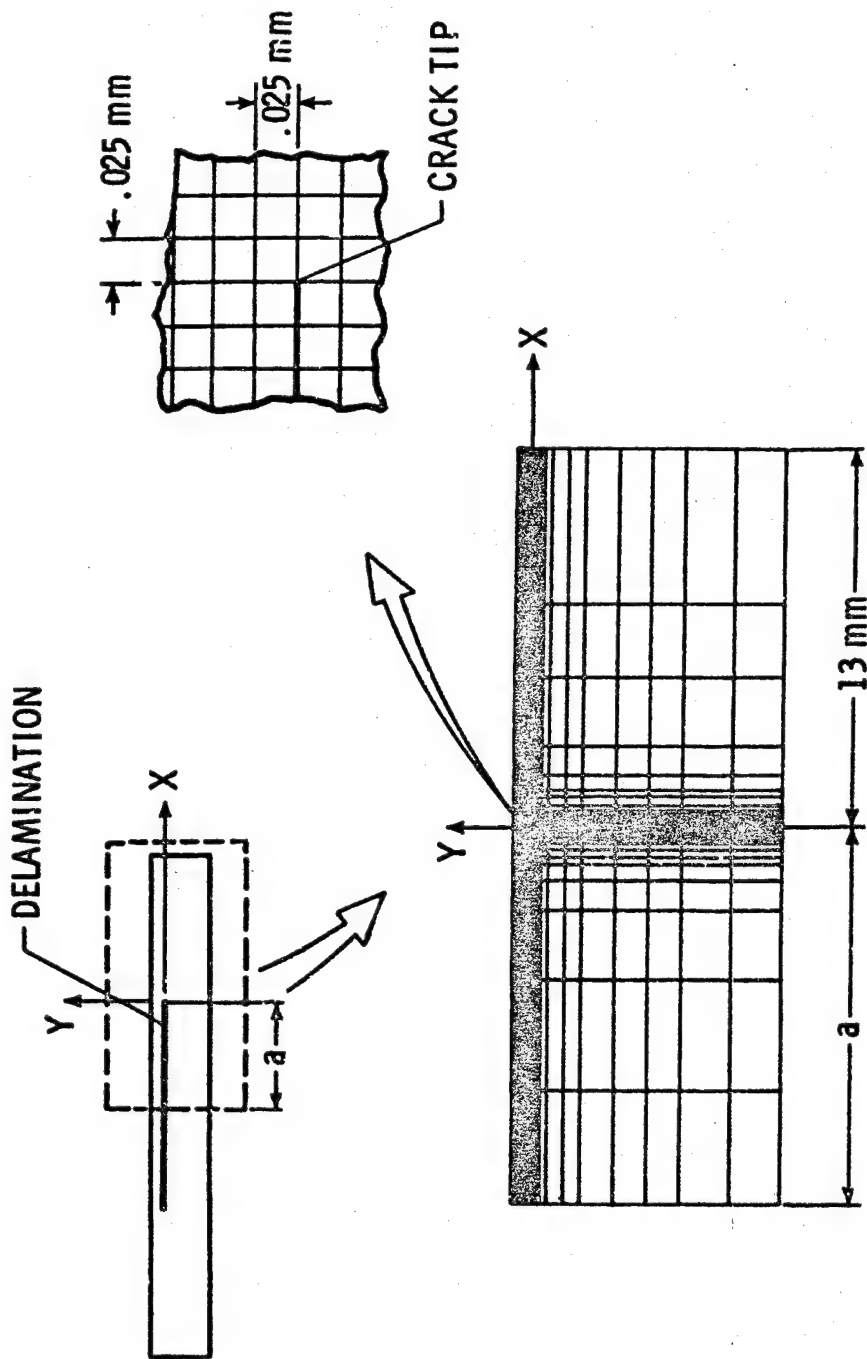
Fig. 3— Typical finite element mesh.
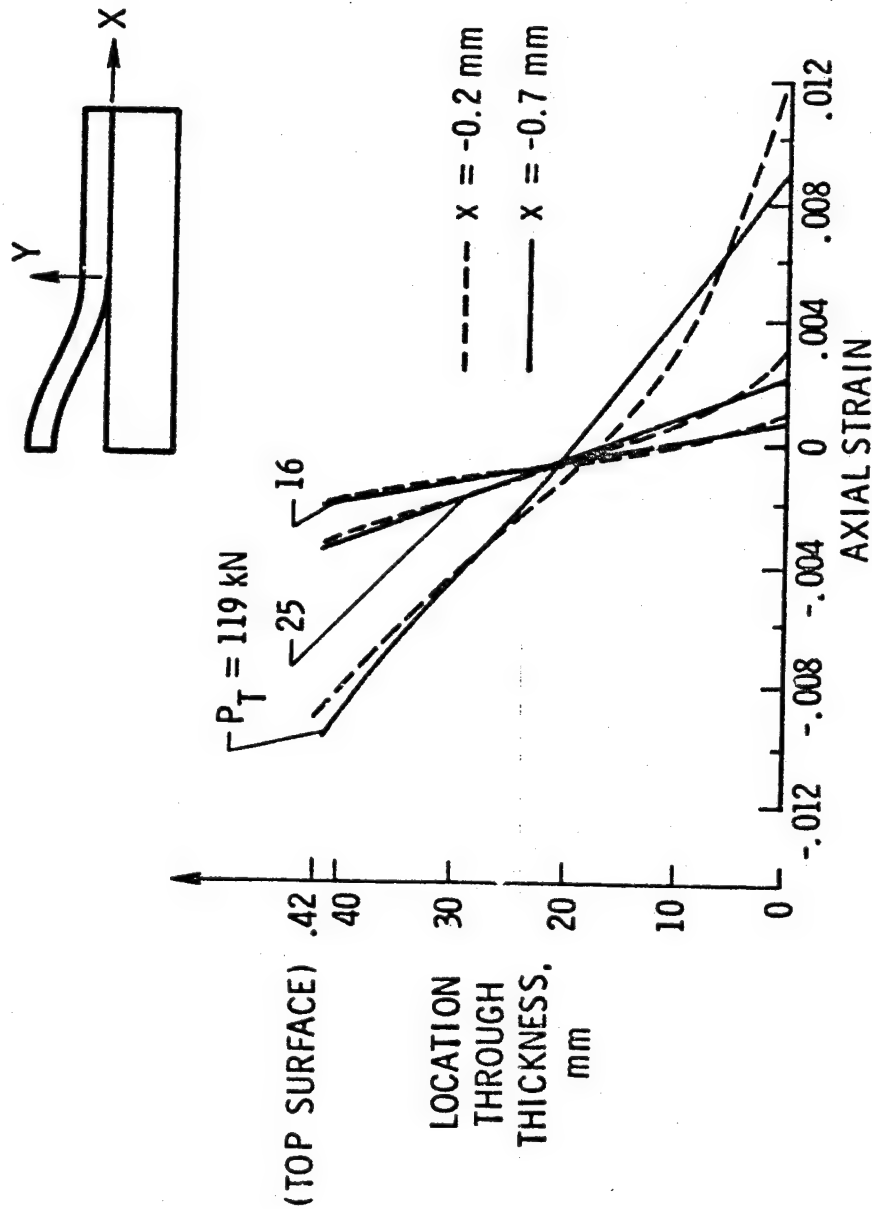
Fig. 4— Variation of axial strain through thickness of buckled region (2a = 25 mm), nonlinear analysis.

25
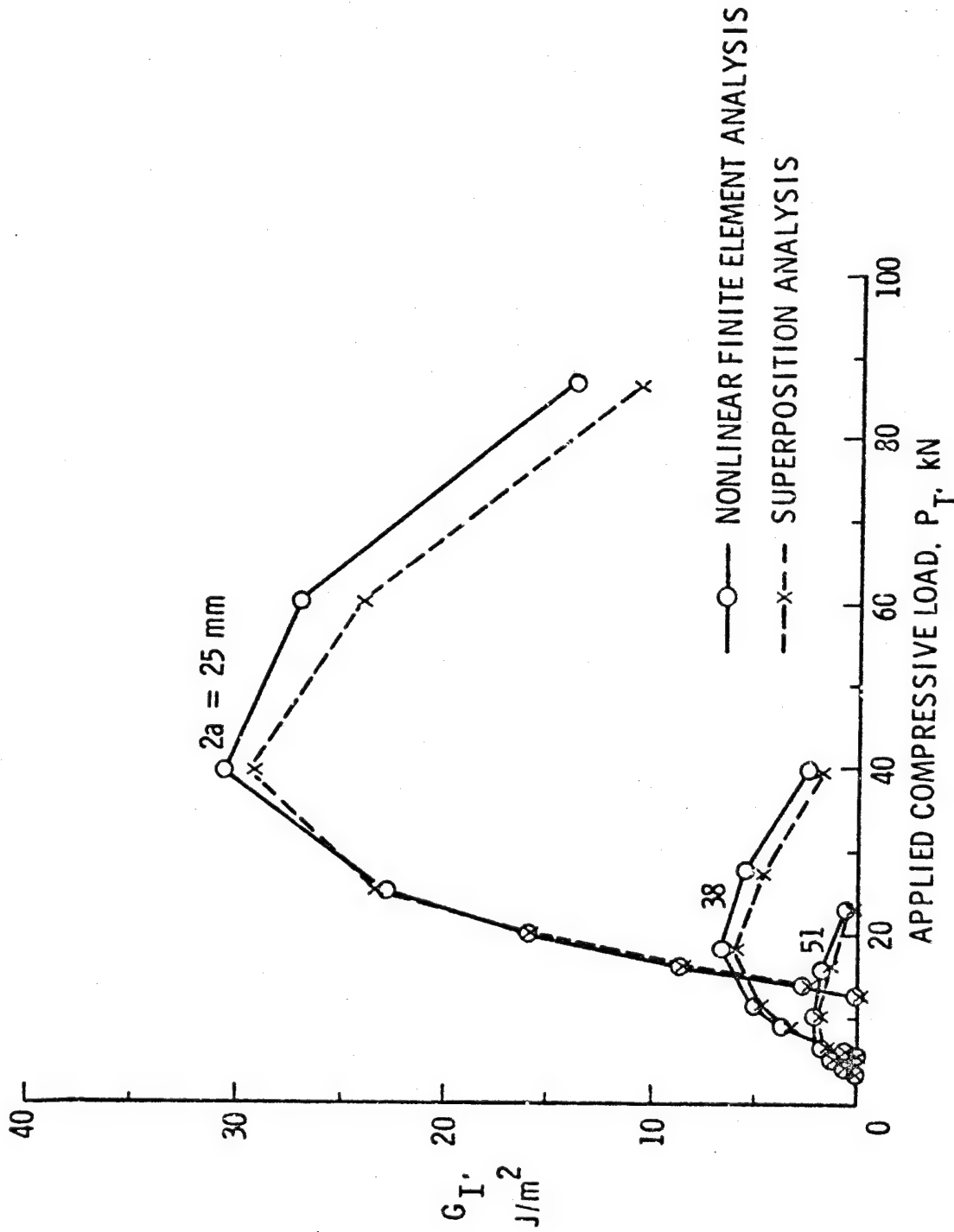
Fig. 5— Evaluation of approximate superposition analysis ($(P_C - P_D)$ and M from nonlinear finite element analysis).
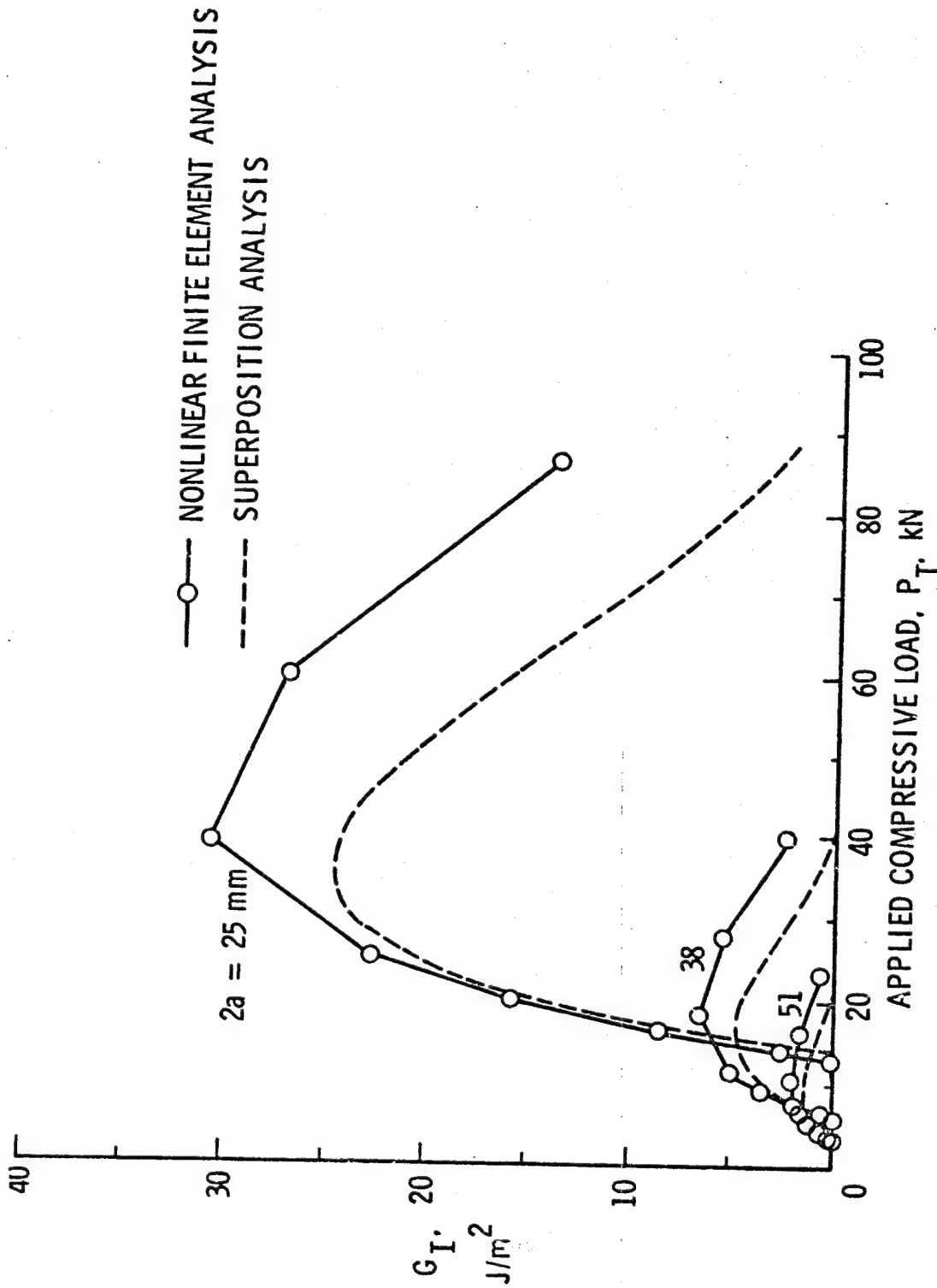
Fig. 6— Evaluation of approximate superposition analysis (($P_C - P_D$) and M from strength of materials analysis).
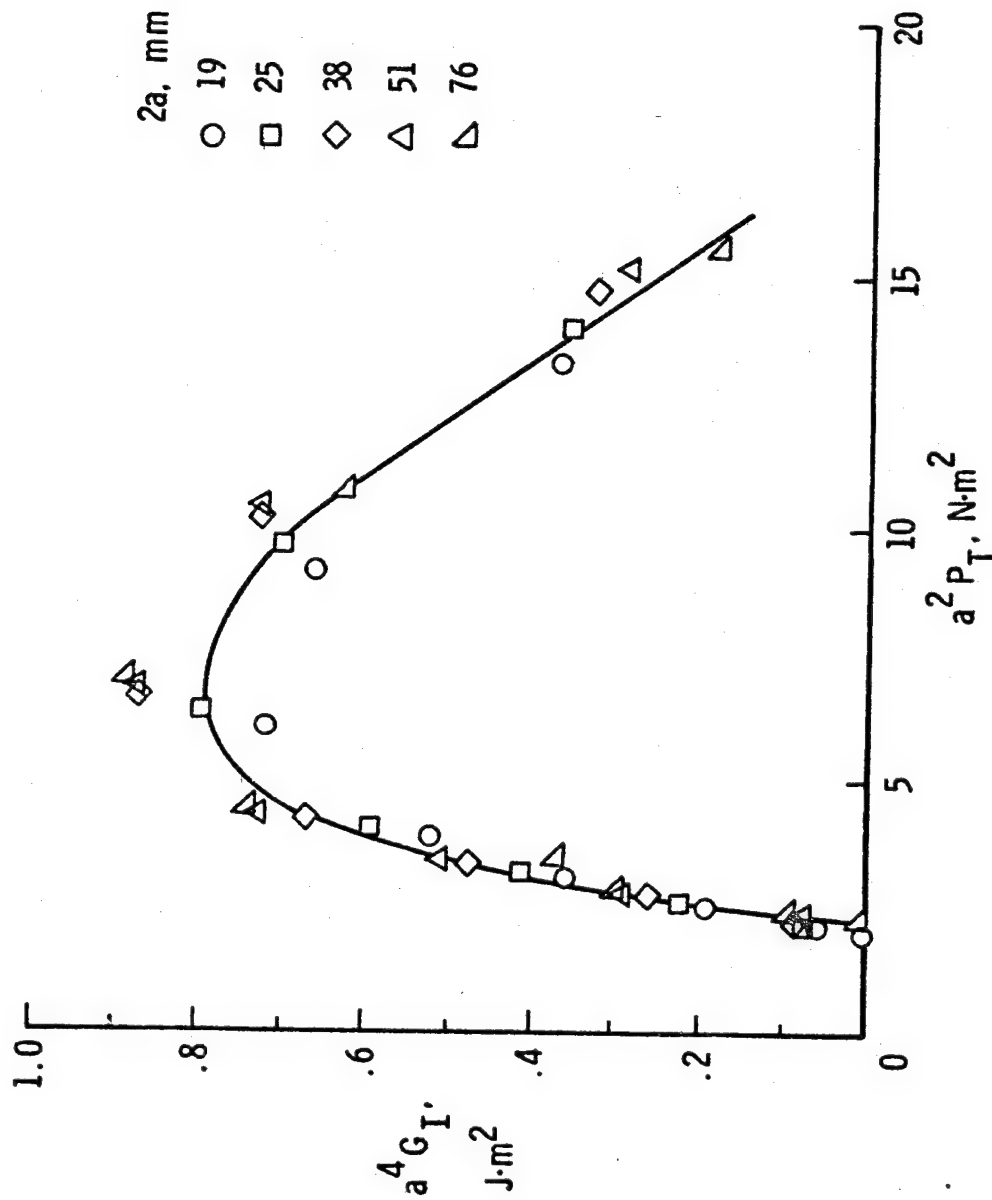
Fig. 7– Compaction of results from geometrically nonlinear analysis. (Curve is visual fit of data.)
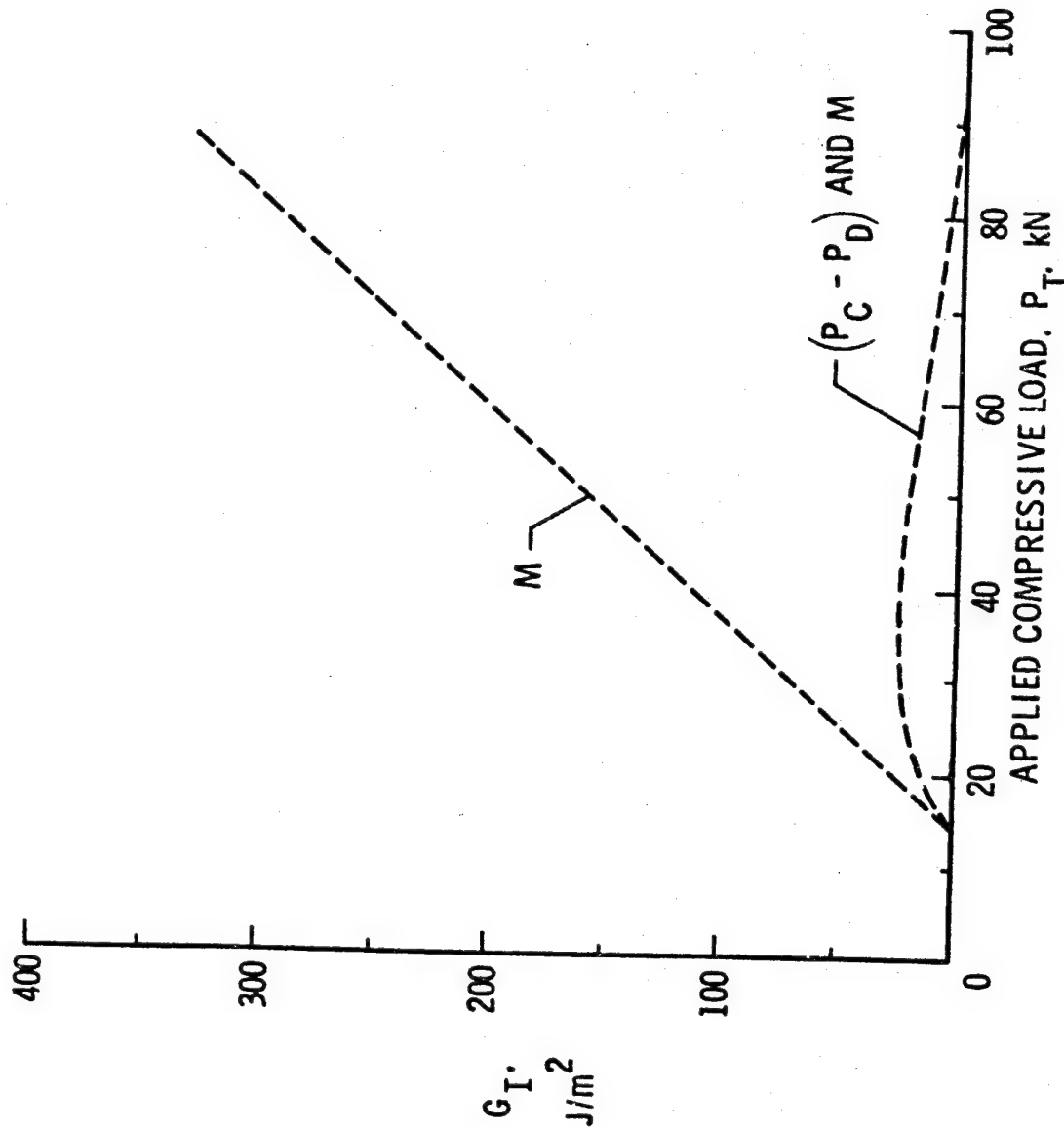
Fig. 8— Effect of $(P_C - P_D)$ and M on G_I (2a = 25 mm).

29
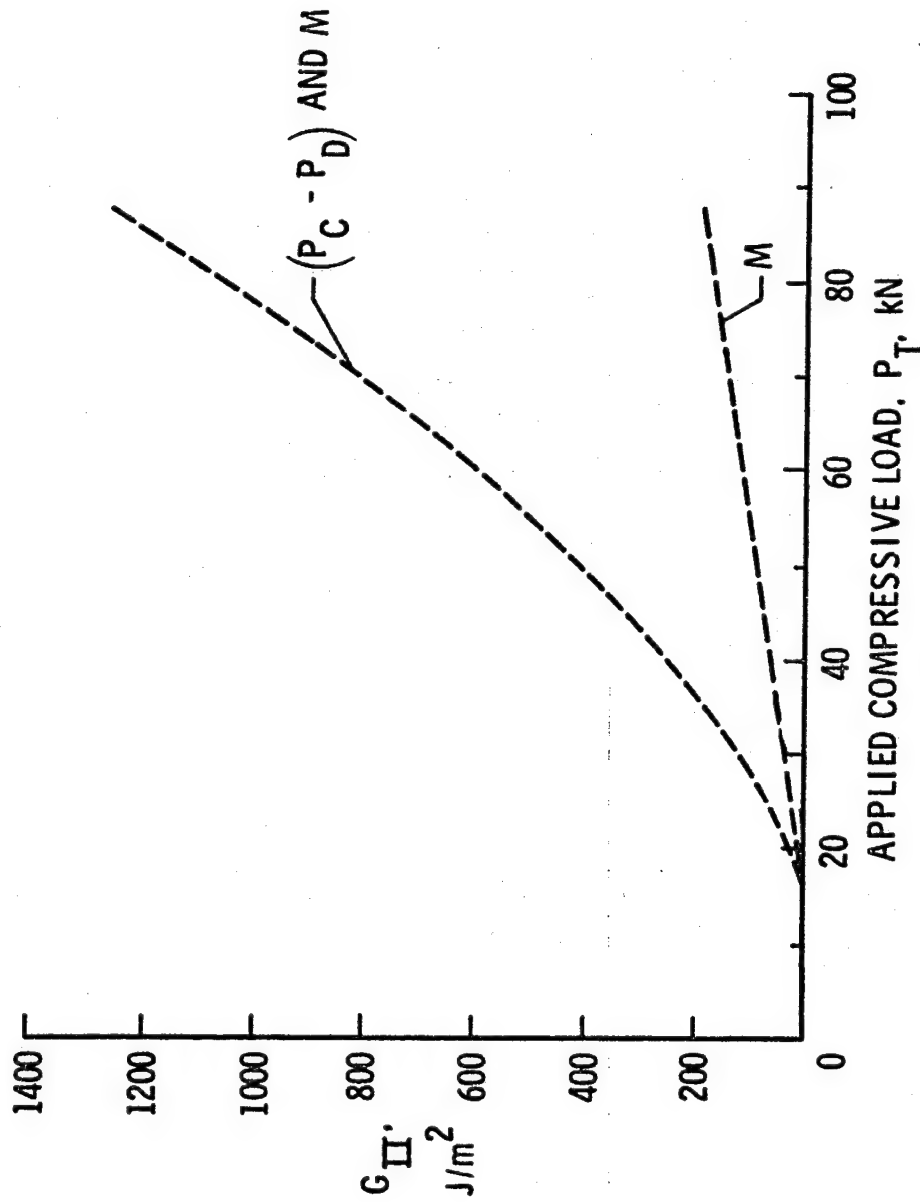
Fig. 9— Effect of $(P_C - P_D)$ and M on G_{II} $(2a = 25$ mm$)$.
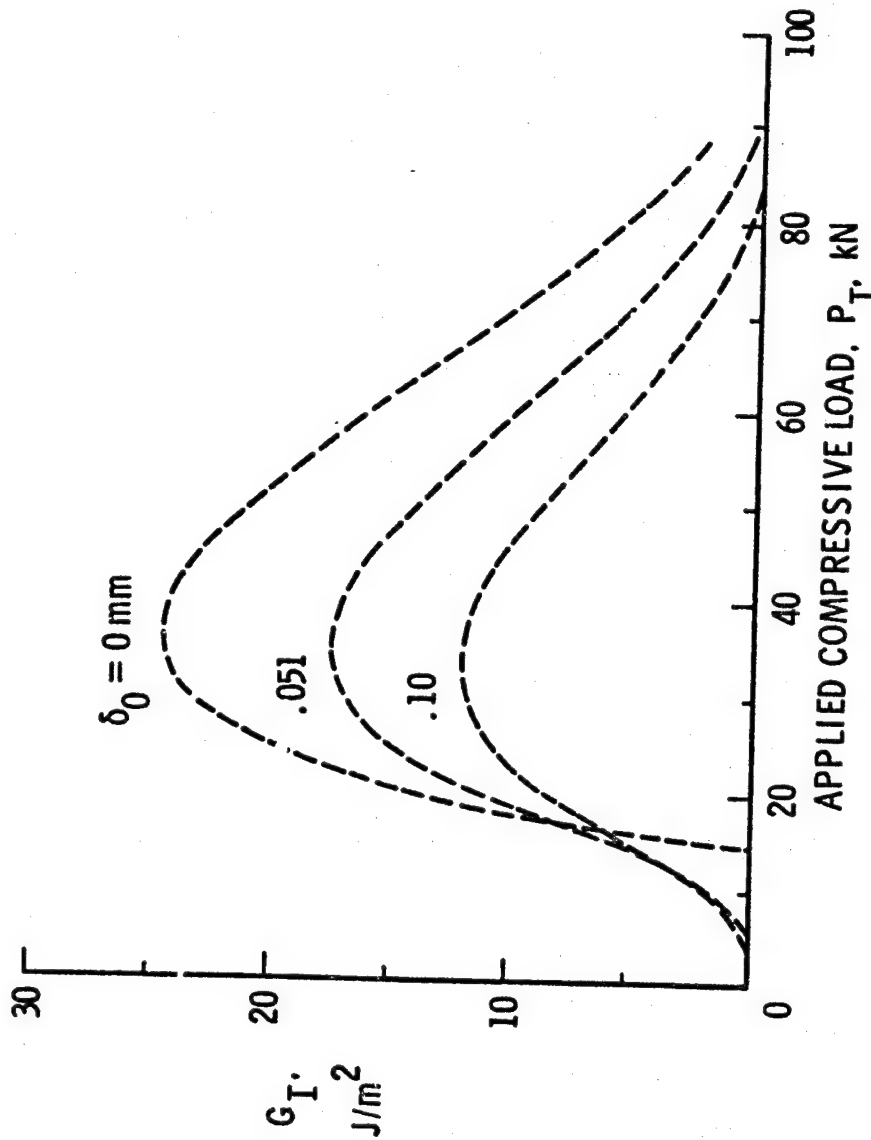
30

Fig. 10— Effect of initial imperfection δ_o on G_I (2a = 25 mm).

31

Fig. 11— Effect of initial imperfection δ_o on G_{II} (2a = 25 mm).

32
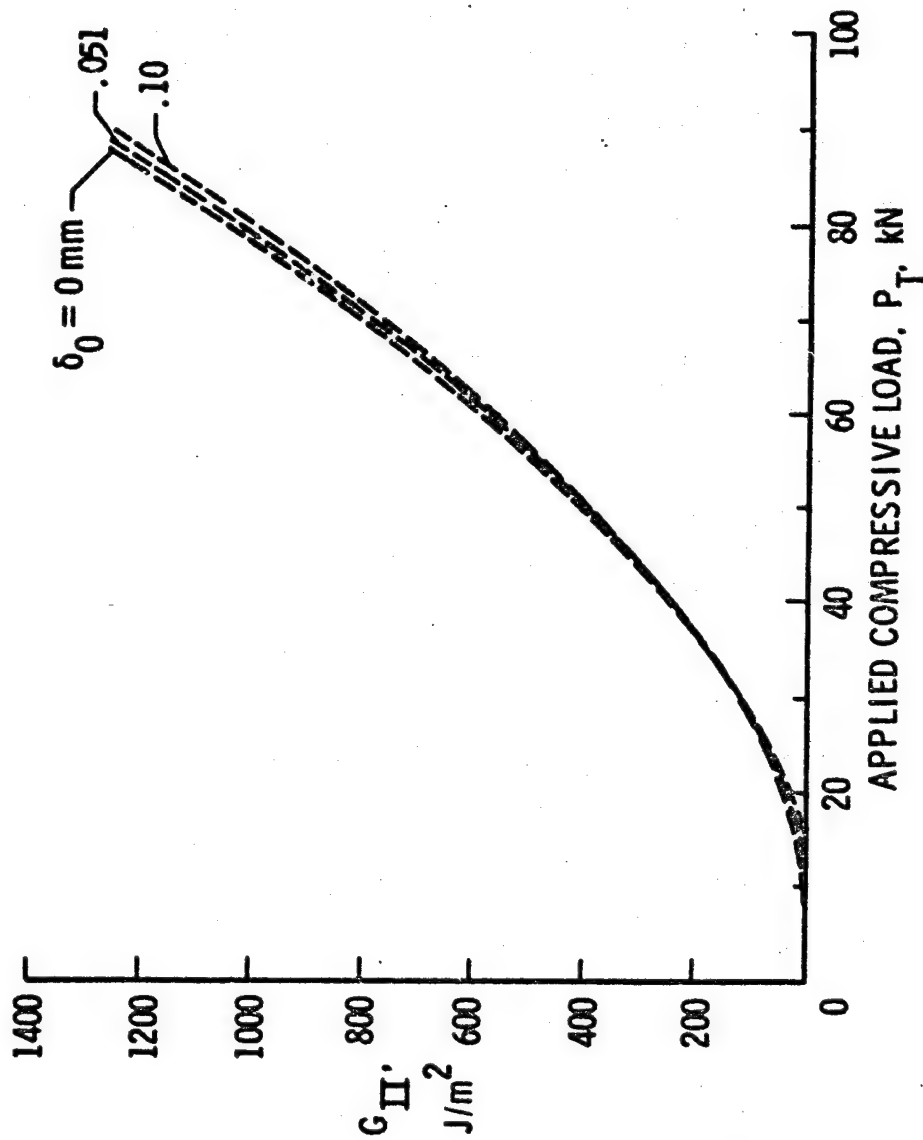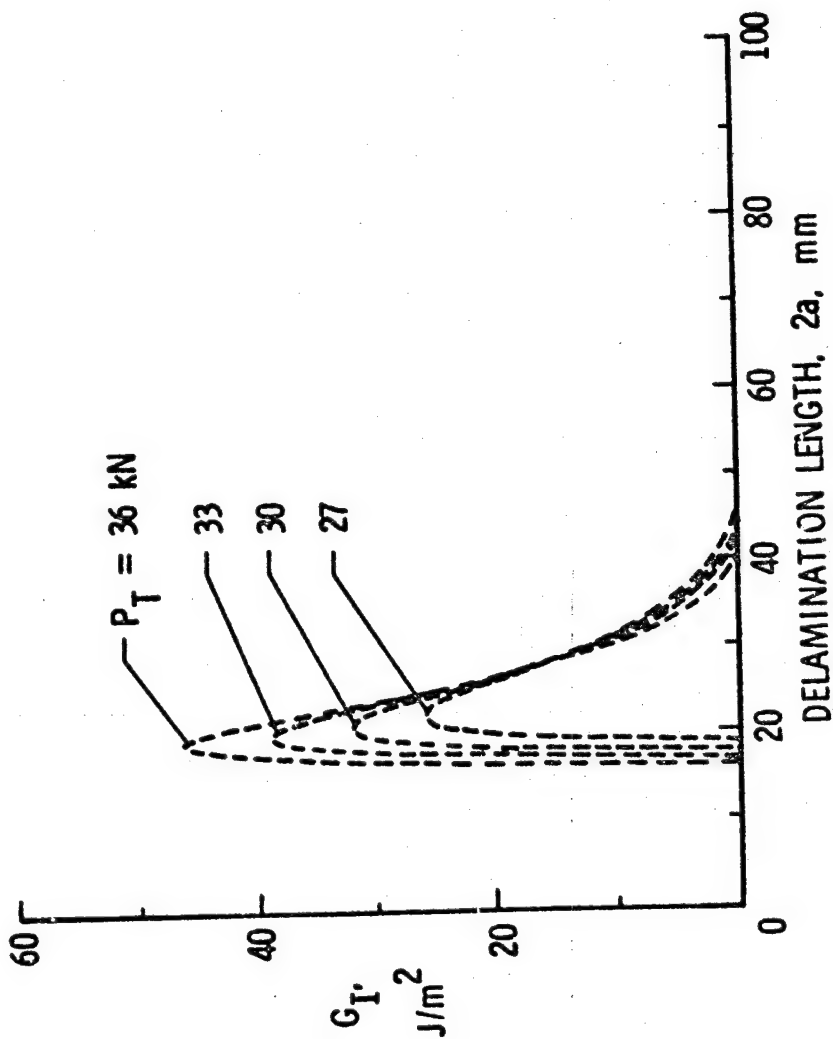
Fig. 12— Effect of delamination length on G_I.
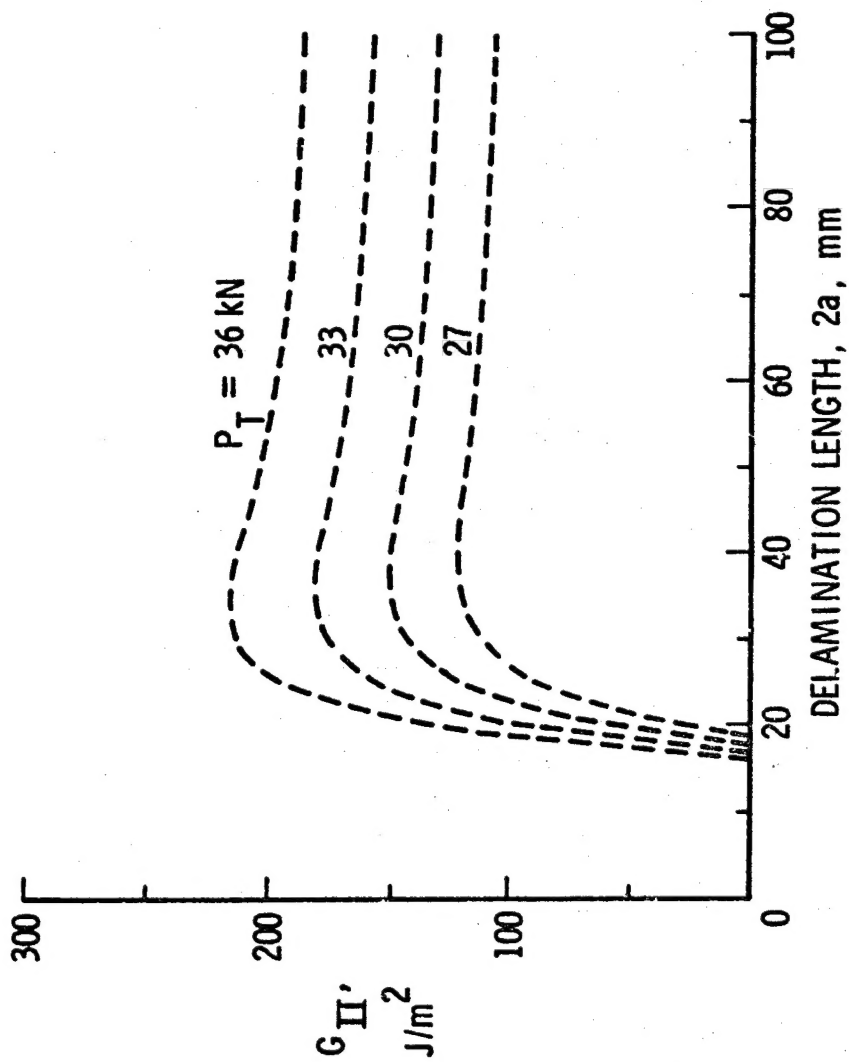
Fig. 13— Effect of delamination length on G_{II}.
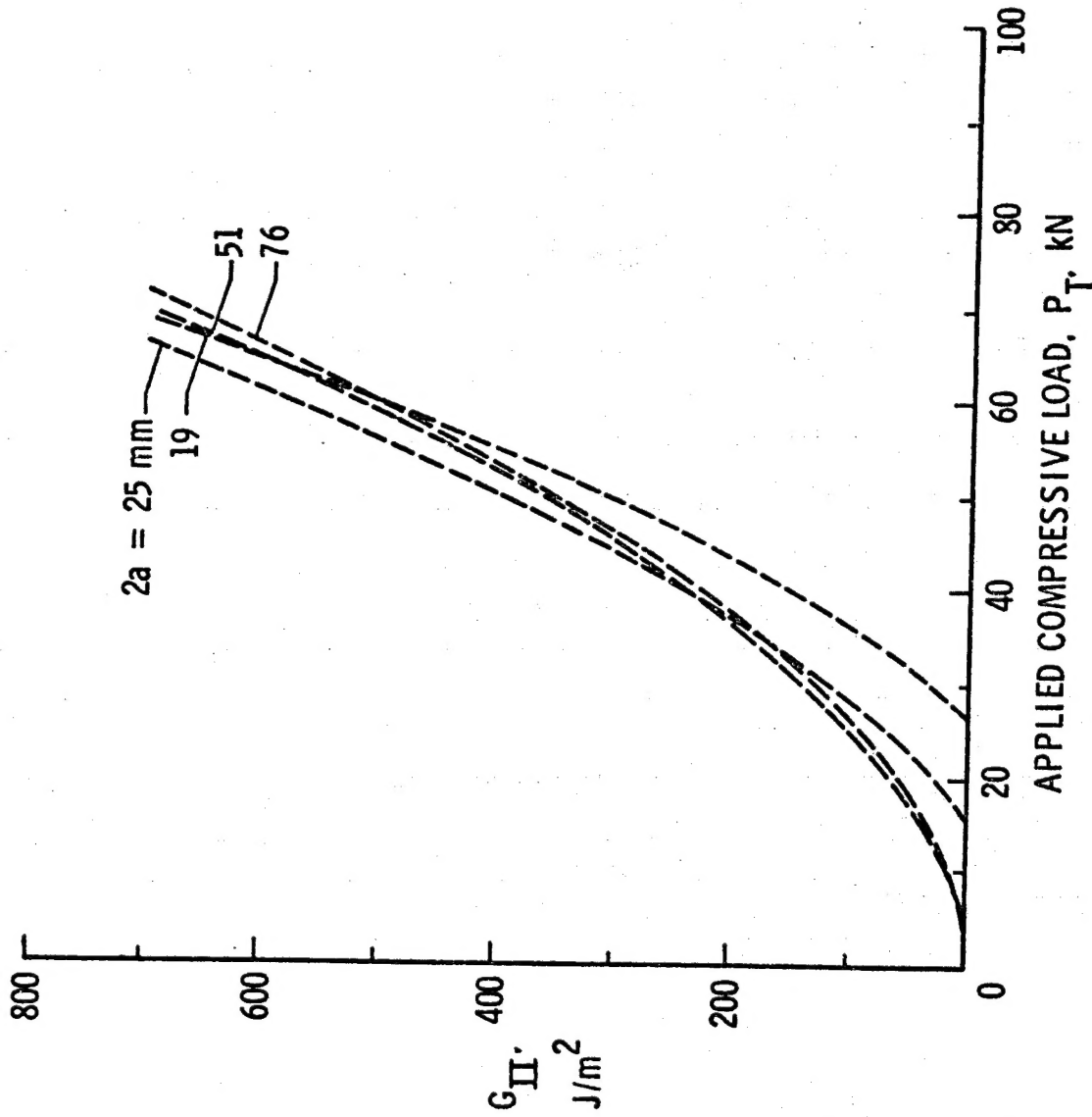
Fig. 14— Effect of applied compressive load on G_{II} ($2a = 25$ mm).

35
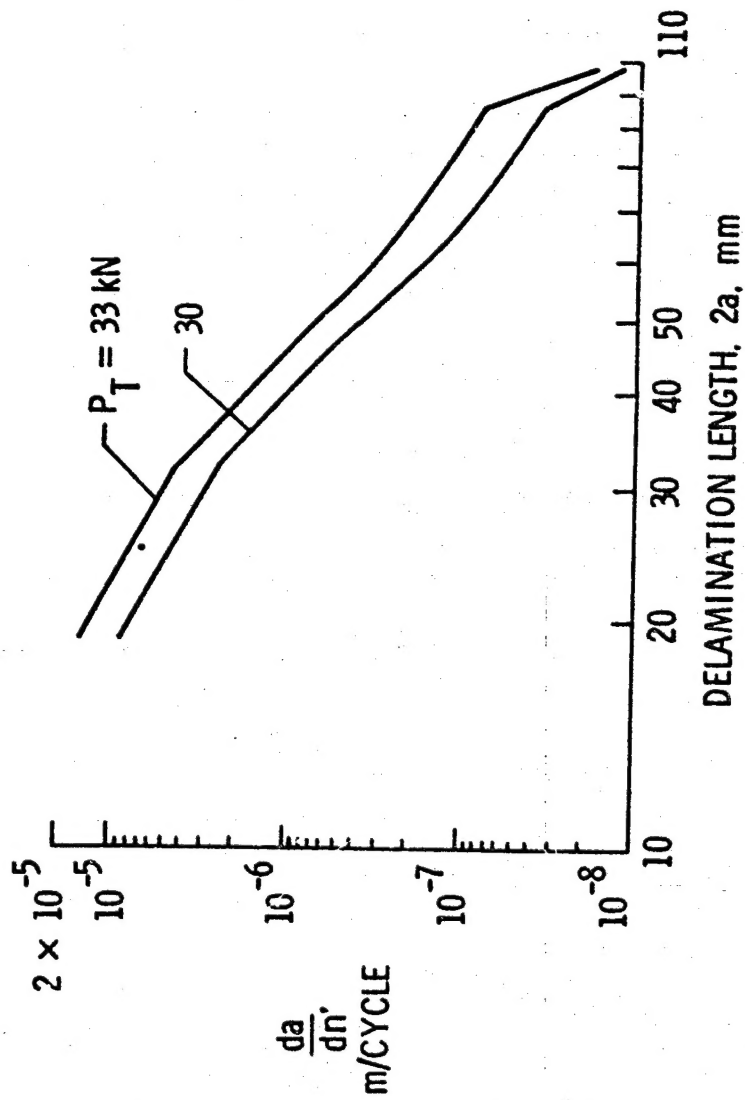
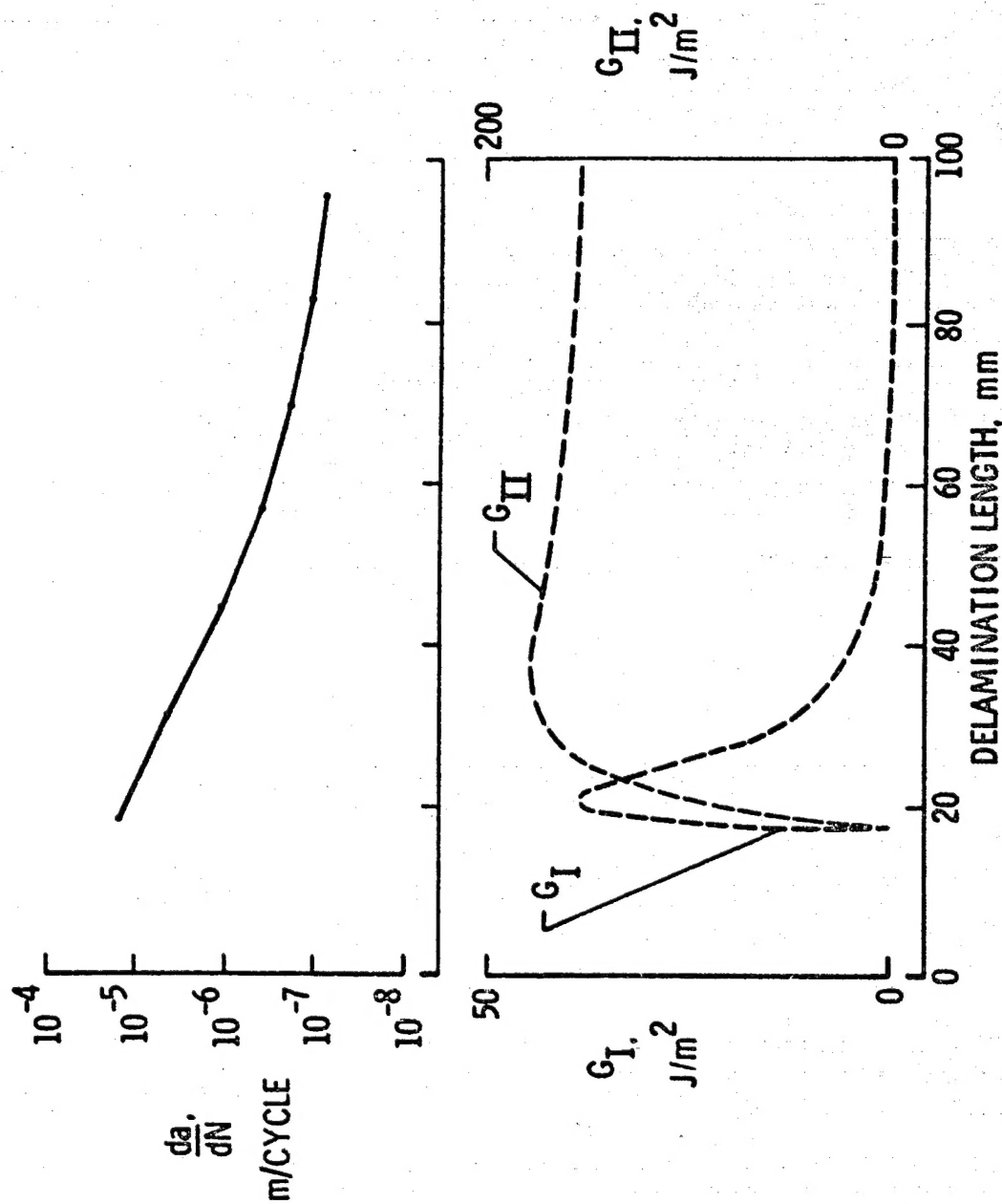Fig. 15— Effect of delamination length and load on growth rate.

Fig. 16— Comparison of G_I, G_{II}, and delamination growth rate for maximum fatigue load of 33 kN.